Cell Reports

Report

The MARCH6-SQLE Axis Controls Endothelial Cholesterol Homeostasis and Angiogenic Sprouting

Graphical Abstract

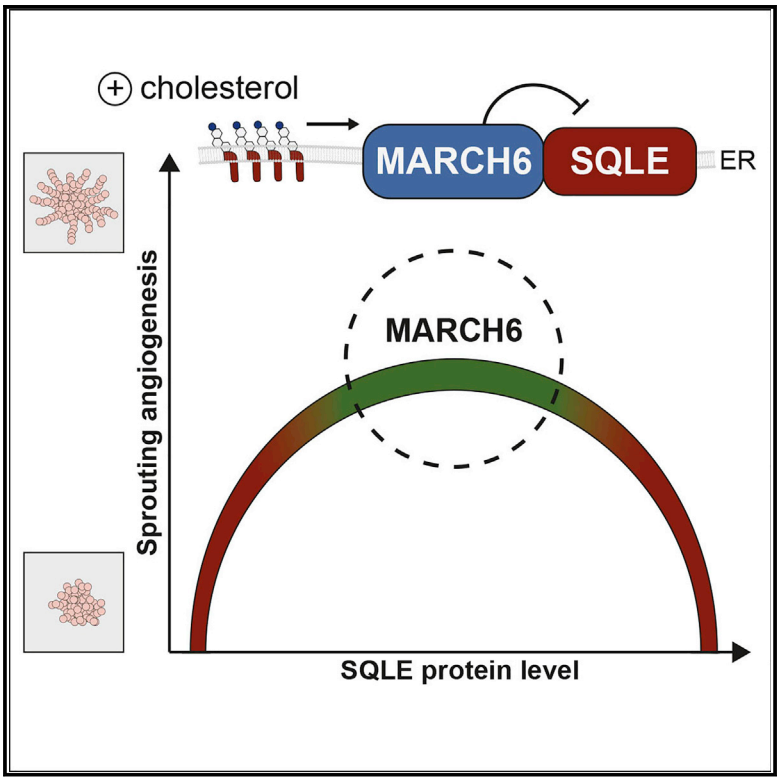

Authors

Josephine Mathilde Elisabeth Tan, Miesje Maxime van der Stoel, Marlene van den Berg, ..., Anke Loregger, Stephan Huveneers, Noam Zelcer

Correspondence

s.huveneers@amsterdamumc.nl (S.H.), n.zelcer@amsterdamumc.nl (N.Z.)

In Brief

Tan et al. identify the E3-ligase MARCH6 as an important regulator of endothelial sprouting angiogenesis, owing to its ability to degrade the cholesterol biosynthetic enzyme SQLE. The study highlights that adequate SQLE levels are a critical determinant of maintaining endothelial junctions and proper sprouting angiogenesis.

Highlights

- Regulation of cholesterol synthesis is a determinant of endothelial function
- MARCH6 governs endothelial cholesterol homeostasis by promoting degradation of SQLE
- MARCH6 loss impairs VE-cadherin-based adherens junctions and sprouting angiogenesis
- Angiogenesis is dependent on fine-tuning SQLE levels in endothelial cells

Tan et al., 2020, Cell Reports *32*, 107944
August 4, 2020
https://doi.org/10.1016/j.celrep.2020.107944

CellPress

Cell Reports

CellPress
OPEN ACCESS

Report

The MARCH6-SQLE Axis Controls Endothelial Cholesterol Homeostasis and Angiogenic Sprouting

Josephine Mathilde Elisabeth Tan,[1,5] Miesje Maxime van der Stoel,[1,5] Marlene van den Berg,[1] Nienke Marlies van Loon,[1] Martina Moeton,[1] Edwin Scholl,[2] Nicole Neeltje van der Wel,[2] Igor Kovačević,[3,4] Peter Lodewijk Hordijk,[3] Anke Loregger,[1] Stephan Huveneers,[1,6,*] and Noam Zelcer[1,6,7,*]

[1]Department of Medical Biochemistry, Amsterdam University Medical Centers, Amsterdam Cardiovascular Sciences, Amsterdam Gastroenterology and Metabolism, University of Amsterdam, Meibergdreef 9, 1105AZ Amsterdam, the Netherlands
[2]Department of Medical Biology, Electron Microscopy Center Amsterdam, Amsterdam UMC, Meibergdreef 9, 1105AZ Amsterdam, the Netherlands
[3]Department of Physiology, Amsterdam University Medical Centers, location VUmc, Amsterdam, the Netherlands
[4]Institute for Physiological Chemistry, Medical Faculty, Martin Luther University Halle-Wittenberg, Hollystrasse 1, 06114 Halle, Germany
[5]These authors contributed equally
[6]Senior authors
[7]Lead Contact
*Correspondence: s.huveneers@amsterdamumc.nl (S.H.), n.zelcer@amsterdamumc.nl (N.Z.)
https://doi.org/10.1016/j.celrep.2020.107944

SUMMARY

The endothelial monolayer forms a barrier between the lumen of blood vessels and the underlying tissues. Stable VE-cadherin-based adherens junctions are essential for maintaining this barrier, whereas their remodeling is required for angiogenesis in health and disease. Here, we position the ERAD-associated ubiquitin ligase MARCH6 as a determinant of angiogenic sprouting and barrier integrity through its ability to promote the degradation of the rate-limiting cholesterol biosynthetic enzyme squalene epoxidase (SQLE). Accordingly, *MARCHF6* ablation in endothelial cells increases SQLE protein and cholesterol load. This leads to altered membrane order, disorganized adherens junctions, decreased endothelial barrier function, and impaired SQLE-dependent sprouting angiogenesis. Akin to *MARCHF6* silencing, the overexpression of *SQLE* impairs angiogenesis. However, angiogenesis is also attenuated when *SQLE* is silenced, indicating that fine-tuning cholesterol biosynthesis is a determinant of healthy endothelial function. In summary, we propose a mechanistic link between regulation of cholesterol homeostasis by the MARCH6-SQLE axis and endothelial integrity and angiogenesis.

INTRODUCTION

Blood vessels are lined by a monolayer of endothelial cells (ECs) that forms a selective barrier between the lumen and underlying tissue (Dejana and Orsenigo, 2013; Vestweber et al., 2009). This barrier relies on the formation of adherens and tight junctions between adjacent ECs so that macromolecules cannot traverse the vessel wall. Accordingly, remodeling of the endothelial barrier is critical in, among others, (patho)physiologic angiogenesis, immune cell trafficking, vascular wound healing, and the onset of atherosclerosis (Carmeliet and Jain, 2011; Vestweber et al., 2009; Weis, 2008)

The breakdown of the endothelial barrier can be triggered by external insults that impinge on the function of ECs (Dejana and Orsenigo, 2013). The detrimental effect of inflammatory signaling (e.g., tumor necrosis factor α [TNF-α], interleukin-1β [IL-1β]) on the endothelial barrier is well documented and is considered one of the early instigating events in the development of atherosclerosis (Hansson and Libby, 2006; Libby, 2002). Similarly, mechanic insults (e.g., turbulent blood flow, age-related vessel stiffening) and perturbation of mechanosensing in ECs are important triggers for the development of cardiovascular disease (Conway and Schwartz, 2013; Hahn and Schwartz, 2009; Li et al., 2019). However, next to external insults, there is mounting evidence pointing toward pathways that govern cellular bioenergetics as important regulators of EC function (Davignon and Ganz, 2004; De Bock et al., 2013; Pober et al., 2009; Schoors et al., 2014). Notably, metabolic reprogramming between the preferential use of fatty acids or glucose by ECs plays an important role in establishing the tip- and stalk-cell phenotype during angiogenesis (Cruys et al., 2016). In addition, ablation of the glycolytic activator PFKFB3 attenuates glycolytic capacity in ECs, and as a result, establishment of endothelial barrier function, the tip-cell phenotype, and angiogenic sprouting *in vivo* (De Bock et al., 2013). However, next to glycolysis, the remodeling and expansion of cellular membranes and the availability of adequate lipids for these processes are required to support vascular sprouting (Li et al., 2019).

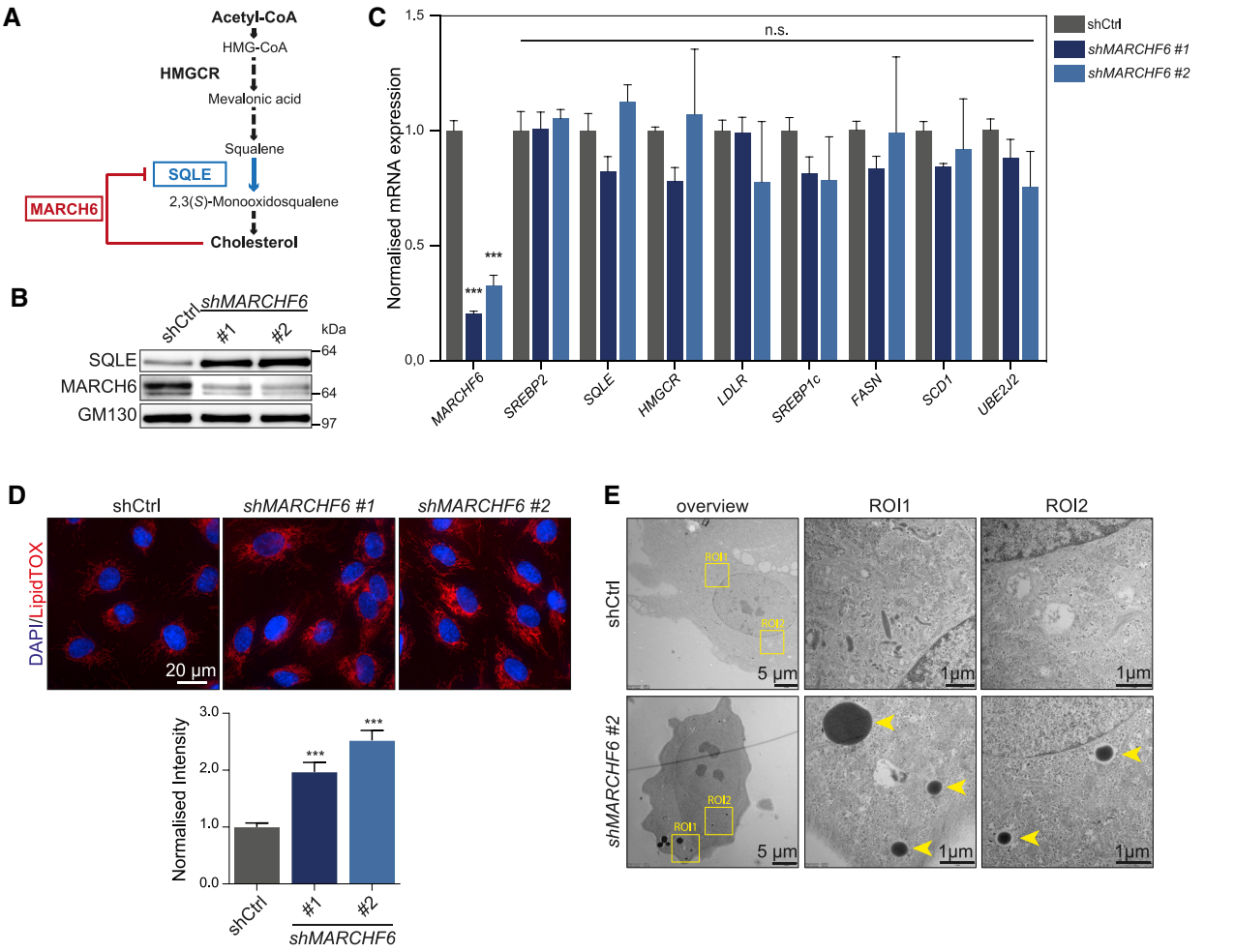

(legend on next page)

Cholesterol is a major lipid constituent of biological membranes and plays a critical role in cellular processes such as intracellular transport, cell signaling, adhesion, membrane fluidity, and permeability (Fang et al., 2013; Gu et al., 2019). Accordingly, enhanced cholesterol efflux to ApoA-1-containing high-density lipoprotein (HDL) in ECs leads to the impaired formation of cholesterol- and sphingomyelin-rich membrane domains (Ikonen, 2001), which reduces angiogenic capacity due to the decreased vascular endothelial growth factor (VEGF) receptor 2 signaling in tip cells (Fang et al., 2013; Gu et al., 2019). However, the role of HDL and cholesterol efflux may be context dependent, as some studies have reported that HDL can also promote angiogenesis (Jin et al., 2018; Tan et al., 2014). The integrity of the endothelium and angiogenesis are governed by, among others, transmembrane cell-cell adhesion molecules such as VE-cadherin. The function of these molecules depends on the organization and fluidity of the plasma membrane, which is sensitive to changes in cholesterol content (Baumgartner et al., 2014). Whereas the role of cholesterol efflux pathways in ECs has received much attention, the contribution of cholesterol biosynthesis to ECs has been largely overlooked. We therefore hypothesized that the regulators of this process could affect endothelial integrity and function.

To explore the role of (dysregulated) cholesterol synthesis on EC function, we studied the consequences of the ablation of the E3-ubiquitin ligase membrane-associated RING-CH 6 (MARCH6), encoded by the *MARCHF6* gene. We have previously shown that MARCH6, an endoplasmic reticulum-associated degradation (ERAD) E3 ligase (Hassink et al., 2005), mediates the cholesterol-dependent degradation of squalene epoxidase (SQLE) (Gill et al., 2011; Loregger et al., 2015; Zelcer et al., 2014). SQLE is a rate-limiting enzyme in the cholesterol biosynthesis pathway and is the enzyme that ultimately commits the pathway to producing cholesterol (Figure 1A). We report here that the MARCH6-SQLE nexus has profound effects on EC integrity and dynamics, which reveals the regulation of cholesterol levels by the ERAD system as a previously unrecognized determinant of EC function.

RESULTS

MARCH6 Governs SQLE and Cholesterol Levels in ECs

SQLE is a rate-limiting enzyme in the synthesis of cholesterol, and its sterol-dependent regulation by MARCH6 serves to control cholesterol synthesis by the mevalonate pathway (Figure 1A) (Sharpe and Brown, 2013; Sharpe et al., 2014; Zelcer et al., 2014). To study the role of MARCH6 and cholesterol biosynthesis in ECs, we interrogated the consequence of its silencing in human umbilical vein endothelial cells (HUVECs), an established primary EC model, using two independent short hairpin RNA (shRNA) constructs. Effective silencing of *MARCHF6* resulted in a marked post-transcriptional increase of its ubiquitylation target SQLE (Figures 1B and 1C). SQLE is also subject to transcriptional regulation by the sterol regulatory element-binding protein (SREBP) transcription factors. However, in line with MARCH6 controlling a post-transcriptional event, the increase in SQLE was not associated with a global increase in the expression of SREBP target genes in these cells (*HMGCR*, *SQLE*, *LDLR*, *SCD1*, and *FASN*) or of *SREBP1* and *SREPB2* themselves (Horton et al., 2003) (Figure 1C). Consistent with this, we also did not observe changes in low-density lipoprotein (LDL) uptake, a close proxy of LDL receptor (LDLR) levels and function (Figure S1A). Similarly, we did not observe a change in the expression of the E2 ubiquitin conjugating enzyme UBE2J2, which we have recently shown to be the cognate E2 used by MARCH6 to promote SQLE ubiquitylation (Loregger et al., 2020; Tan et al., 2019). These results are in line with the post-transcriptional regulation of SQLE by MARCH6 in ECs, as we and others have observed in other model cell systems (Chua et al., 2019; Gill et al., 2011; Loregger et al., 2015; Zelcer et al., 2014). The loss of MARCH6 was associated with an increase in neutral-lipid accumulation compared to control cells (Figure 1D). In electron micrography images, we readily observed lipid accumulation in lipid droplet structures (Figure 1E), with no overt alterations in cellular organelles or structures such as endosomes or mitochondria upon MARCH6 loss. Given the elevated levels of SQLE in cells lacking MARCH6, we reasoned that this may result in increased cellular cholesterol content. We measured an

Figure 1. MARCH6 Governs SQLE and Cholesterol Levels in Endothelial Cells

(A) Schematic representation of the mevalonate pathway depicting the rate-limiting enzymes HMGCR and SQLE. MARCH6 promotes the cholesterol-stimulated ubiquitylation and subsequent degradation of SQLE.

(B) HUVECs were transduced with shCtrl, *shMARCHF6* #1, or *shMARCHF6* #2. Subsequently, cellular membranes were isolated and immunoblotted as indicated. GM130 acts as a loading control. The immunoblot is representative of at least 3 independent experiments.

(C) HUVECs were treated as in (B), and gene expression of the indicated genes was determined by qPCR. Each bar represents the mean ± SE normalized to shCtrl. n = 3, n.s., non-significant, ***p < 0.001.

(D) Cells were stained with LipidTox to identify lipid droplets. A representative immunofluorescence (IF) image of the indicated cells and quantification is shown. Each bar represents the mean intensity ± SE. The signal is corrected for background and normalized to shCtrl. n = 3, ***p < 0.001.

(E) Representative electron microscopy images of HUVECs transduced with shCtrl or *shMARCHF6* #2. The arrows indicate lipid droplets. Overview image: 2,900× magnification. Boxed region of interest: 23,000× magnification.

(F) HUVECs were treated as in (B), and cellular lipids were extracted and cholesterol content determined using the Amplex Red assay. The bar graph represents the means ± SEs normalized to shCtrl. n = 3, *p < 0.05.

(G) HUVECs were transduced with the indicated constructs and subsequently stained with filipin to mark cellular-free cholesterol. Representative widefield IF images and quantification are shown. Each bar represents the mean intensity ± SE. The signal is corrected for background and normalized to shCtrl. n = 3, ***p < 0.001, **p < 0.01.

(H) Representative images of HUVECs transduced with either shCtrl, *shMARCHF6* #1 and *shMARCHF6* #2 stained with laurdan. The images are pseudocolored according to the GP value, as specified in the lookup table.

(I) Quantification of the relative changes in membrane order (GP) normalized to shCtrl. Each bar represents the mean intensity ± SE. n = 3, ***p < 0.001.

(J) Expression of *MARCHF6* in laurdan experiments. Each bar represents the mean ± SE normalized to shCtrl. n = 3, **p < 0.01.

increase in total cellular cholesterol when MARCH6 was silenced (Figure 1F). Using filipin, an established cellular dye that specifically marks free cholesterol, we observed a marked difference in the level of free cholesterol in *MARCHF6*-silenced cells (Figure 1G). Not only was there an apparent increase in total filipin signal, but there was also an increased signal at the plasma membrane interface between neighboring ECs. To evaluate whether the MARCH6-induced changes in lipid homeostasis influence the biophysical properties of cellular membranes, we resorted to using laurdan, a dye whose fluorescence reports on membrane polarity and order (Owen et al., 2011). These experiments show that membrane order is decreased in *MARCHF6*-silenced ECs (i.e., the generalized polarization [GP] value is lower) (Figures 1H–1J). These experiments indicate that MARCH6 specifically regulates SQLE levels and that the loss of this regulatory node disrupts cellular cholesterol homeostasis and membrane properties.

Disorganization of VE-Cadherin-Based Cell-Cell Junctions by MARCHF6 Silencing

To achieve their primary role as an endothelial barrier, ECs form adherens junctions that safeguard endothelial integrity (Dejana and Orsenigo, 2013; Vestweber et al., 2009). The plasma membrane receptor VE-cadherin is the key adhesive and structural component of these junctions that connects to the actin cytoskeleton. VE-cadherin is crucial for vascular function and is hence subject to dynamic spatiotemporal regulation (Giannotta et al., 2013; Hahn and Schwartz, 2009). As we observed marked accumulation of cholesterol in the plasma membrane and cell-cell interface of cells lacking MARCH6, we interrogated the level and dynamic distribution of VE-cadherin in ECs. In the absence of MARCH6 the distribution of VE-cadherin at adherens junctions was markedly altered, with a notable widening of the intra-junctional space (Figure 2A). Using the Junction Mapper tool (Brezovjakova et al., 2019) we analyzed the VE-cadherin signal and found a significant decrease in VE-cadherin occupancy and intensity per junctional interface area (Figures 2B and 2C). This was not due to changes in total cellular VE-cadherin levels, as these were unaffected by *MARCHF6* silencing (Figure 2D). A similar junctional pattern was observed when analyzing the cadherin-binding protein β-catenin, further suggesting that while the adherens complex can be formed, the junctions themselves are disorganized (Figures S2A–S2C). In contrast, the number of integrin-based focal adhesions, as assessed by vinculin staining, remained unchanged (Figures S2D and S2E). Since adherens junctions are dynamic structures that undergo continuous remodeling, we next evaluated whether the absence of MARCH6 influences VE-cadherin dynamics. In line with our static images, we observed that while MARCHF6-silenced ECs are able to form VE-cadherin-based junctions, their organization and turnover in time are dramatically different from cell-cell junctions in normal ECs (Figure 2E and Video S1). *MARCHF6*-silenced ECs form long-lived widened and spread VE-cadherin junctional plaques, which were not able to stabilize into mature adhesions, as seen in control ECs. These results indicate that the loss of MARCH6 activity results in the disorganization of VE-cadherin-based adherens junctions.

Disturbed EC Barrier Function and Angiogenic Sprouting in the Absence of MARCH6

The barrier of the endothelium relies on the formation of adherens and tight junctions between neighboring cells. As the silencing of *MARCHF6* leads to disorganized adherens junctions, we assessed whether this affects endothelial barrier function (Giannotta et al., 2013). To determine endothelial barrier formation, we used electric cell-substrate impedance sensing (ECIS) methodology, which provides a quantitative estimate of barrier function. In comparison to control cells, the silencing of *MARCHF6* led to an ~±40% reduction in the resistance of the endothelial barrier (Figure 3A), without affecting cellular viability (Figure S3A). Next to the central role of adherens junctions in forming and maintaining the endothelial barrier, the ability to dynamically remodel these junctions plays a key role during the migration of ECs in (patho)physiological angiogenesis (Bentley et al., 2014; Montero-Balaguer et al., 2009). Accordingly, we observed significantly reduced collective cell migration in *MARCHF6*-silenced cells that was independent of proliferation (Figures 3B and 3C). Angiogenic sprouting can be modeled by determining 3-dimensional sprout formation in a collagen matrix that is induced by the angiogenic growth factor VEGF (Figure 3D). In this model, the silencing of *MARCHF6* reduced not only the number of sprouts but also the cumulative length of those that were formed (Figures 3E–3G). Similarly, impairing the degradation of SQLE by MARCH6 by the knockdown of *UBE2J2,* the cognate E2 ligase in this process (Tan et al., 2019), attenuates VEGF-induced sprouting angiogenesis (Figures S3B–S3F). As such, our results support the notion that the dysregulation of MARCH6 function, which is associated with altered cholesterol homeostasis, reduces the ability of ECs to form an intact barrier and to support VEGF-induced endothelial remodeling during sprouting angiogenesis.

Dysregulation of SQLE Function Underlies MARCH6-Induced EC Dysfunction

Having established that the loss of MARCH6 impairs EC function, we reasoned that this could be due to an increase in SQLE and an inability to control cholesterol synthesis at the level of SQLE. We therefore hypothesized that the overproduction of SQLE by EC would phenocopy the consequence of *MARCHF6* silencing. The overexpression of high levels of SQLE leads to an increase of free cholesterol in EC compared to control (Figures 4A, 4B, S2A, and S2B). Similar to the loss of MARCH6, which results in increased SQLE levels, the overexpression of SQLE markedly attenuated the ability of EC to mediate VEGF-induced sprouting angiogenesis (Figures 4C–4E). These results position SQLE as a regulator of cholesterol homeostasis and EC function. SQLE catalyzes the rate-limiting conversion of squalene to monooxidosqualene in the mevalonate pathway, a reaction that commits the pathway to making cholesterol. To test whether the increase in cellular cholesterol following *MARCHF6* silencing is dependent on SQLE activity, we evaluated the consequence of pharmacological SQLE inhibition with NB-598 (Horie et al., 1990). We observed that treatment with NB-598 reduced free cholesterol accumulation in *MARCHF6*-silenced cells to levels comparable to those seen in control cells (Figures 4F and 4G). Overall, these findings are in line with the

CellPress
OPEN ACCESS

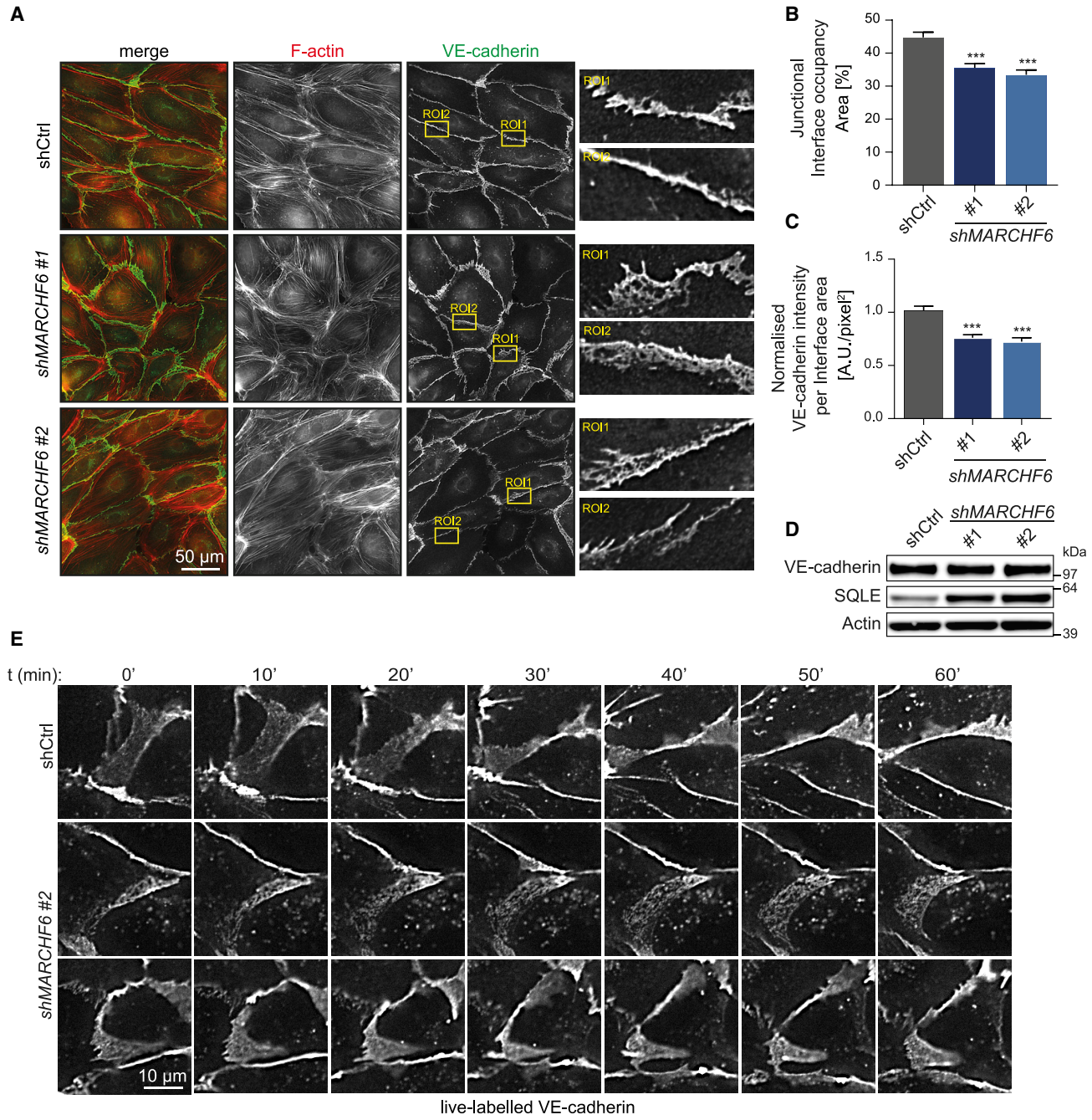

Figure 2. VE-Cadherin-Containing Adherens Junctions Are Disrupted by *MARCHF6* Silencing

(A) HUVECs were transduced as indicated and stained for F-actin (red) and VE-cadherin (green). n = 3.

(B) The mean VE-cadherin interface occupancy ± SE was quantified with the Junction Mapper tool. n = 3. Junctions were analyzed from 51–56 cells per condition. ***$p < 0.001$.

(C) The normalized VE-cadherin intensity per interface area ± SE was quantified with the Junction Mapper tool. n = 3. Junctions were analyzed from 51–56 cells per condition. ***$p < 0.001$.

(D) Cells were treated as in (A), and total cell lysates were immunoblotted as indicated. A representative blot is shown. n = 3.

(E) Still images from time-lapse widefield IF imaging of HUVECs transduced with shCtrl or *shMARCHF6* #2 treated with the Alexa Fluor 647 mouse anti-CD5 antibody. t, minutes. The dashed line shows the junctional area.

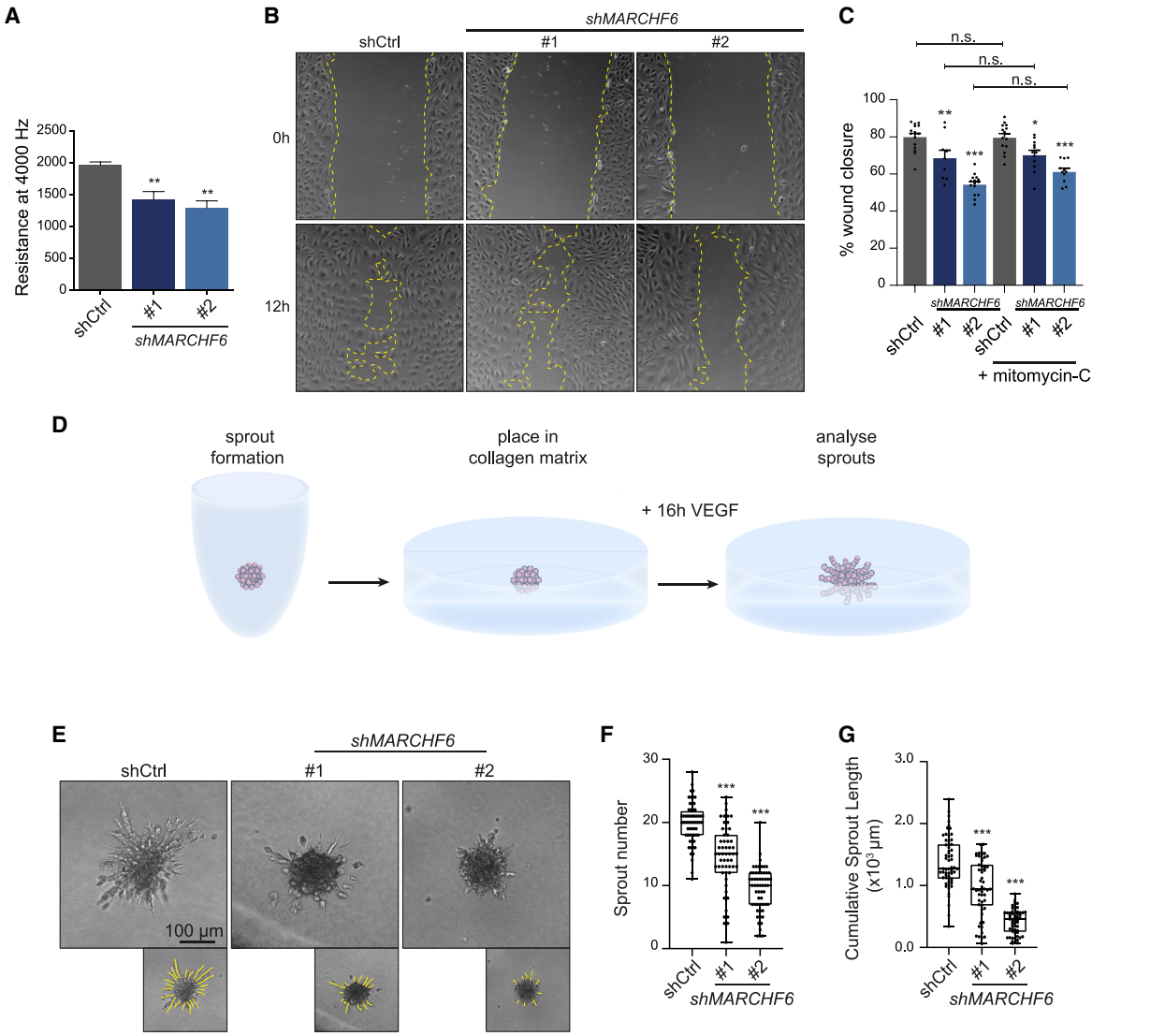

Figure 3. Disturbed EC Barrier Function and Angiogenic Sprouting in the Absence of MARCH6

(A) HUVECs were transduced as indicated, and the barrier resistance at 4,000 Hz was measured using ECIS 24 h after seeding. Each bar shows the average trans-endothelial resistance ± SE. n = 3, ***p < 0.001.

(B) Representative widefield images of HUVECs transduced with the indicated constructs 0 and 12 h after infliction of scratch. The yellow dotted lines mark the wound healing borders.

(C) Bar graph represents the average percentage of wound closure ± SE 12 h after scratch in the indicated cells cultured in the presence or absence of the proliferation inhibitor mitomycin C. n = 3, *p < 0.05, **p < 0.01, ***p < 0.001.

(D) Schematic overview of the VEGF-induced sprouting angiogenesis assay. Briefly, ECs are plated in a U-bottom well plate to form spheroids. Subsequently, spheroids are placed into a collagen matrix and angiogenesis is stimulated with VEGF for 16 h before analysis.

(E) HUVECs were transduced as indicated, and sprouting angiogenesis was stimulated with 50 ng mL^{-1} VEGF for 16 h. Representative phase-contrast images of sprouting spheroids are shown. A total of 60/55/58 spheroids were analyzed for shCtrl, *shMARCHF6* #1, and *shMARCHF6* #2, respectively. n = 4.

(F and G) Boxplot showing the median (±upper and lower quartiles) number of (F) sprouts and (G) cumulative sprout length in the VEGF-induced spheroid-based angiogenesis assays. Whiskers show the minimum and maximum values. n = 4, ***p < 0.001.

hypothesis that enhanced SQLE activity may be the basis for the effect of MARCH6 loss on EC function. To further establish this concept, we tested whether genetic inhibition of SQLE can restore angiogenic sprouting when MARCH6 is absent. The silencing of SQLE was highly effective and resulted in close-to-undetectable SQLE protein in control cells (Figure 4H). As anticipated, the silencing of *MARCHF6* increased SQLE protein abundance, and subsequent silencing of *SQLE* in these cells reverted the level of SQLE to that observed in control cells, with the residual SQLE protein likely reflecting a loss of post-transcriptional regulation by MARCH6 (Figure 4H). Similar to the overproduction of SQLE, lowering SQLE levels in itself largely abolished

CellPress
OPEN ACCESS

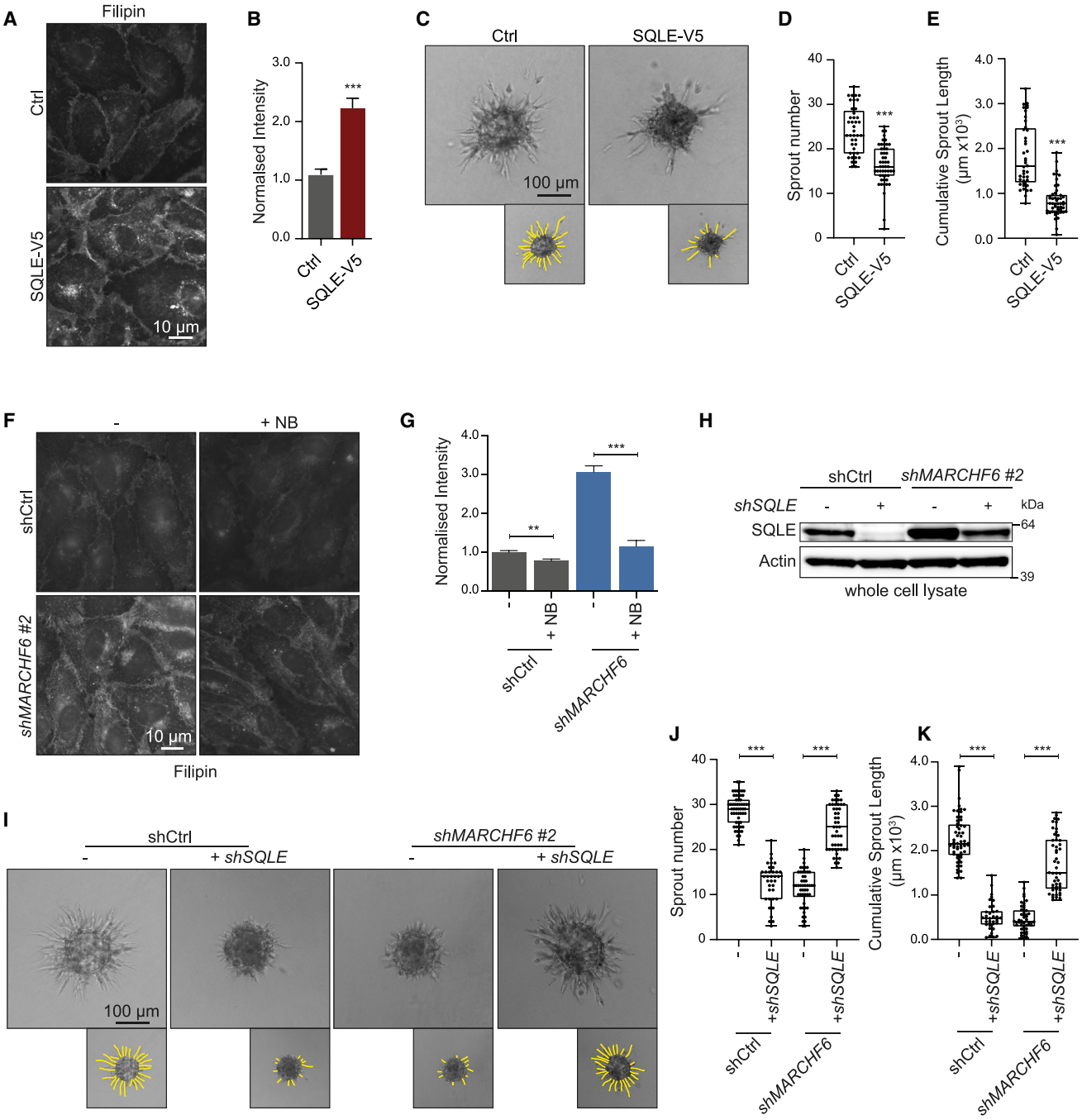

Figure 4. Dysregulation of SQLE Function Underlies MARCH6-Induced EC Dysfunction

Figure360▷ For a Figure360 author presentation of this figure, see https://doi.org/10.1016/j.celrep.2020.107944.

(A and B) HUVECs were transduced with Ctrl or SQLE-V5 encoding constructs, plated on coverslips, and stained with filipin as shown (A), and filipin intensity was quantified (B). Each bar shows the mean filipin intensity ± SE. The signal was corrected for background and normalized to Ctrl. n = 3, ***p < 0.001.

(C) Cells were treated as in (A), and representative phase-contrast images of sprouting spheroids 16 h after VEGF stimulation are shown. A total of 41/50 spheroids were analyzed for Ctrl/SQLE-V5, respectively.

(D) Boxplot showing the median (±upper and lower quartiles) number of sprouts in the spheroid-based angiogenesis assays. Whiskers show the minimum and maximum values. n = 4, ***p < 0.001.

(E) Boxplot showing the median (±upper and lower quartiles) cumulative sprout length in the spheroid-based angiogenesis assays. Whiskers show the minimum and maximum values. n = 4, ***p < 0.001.

(F) Representative IF images of HUVECs transduced with shCtrl or *shMARCHF6 #2* and subsequently treated with DMSO (vehicle) or 2.5 μM NB-589 for 16 h, after which they were stained with filipin III.

(legend continued on next page)

the sprouting capacity of control cells (Figures 4I–4K). However, restoring SQLE levels in MARCH6-depleted cells largely reversed the sprouting angiogenesis defect in these cells and increased both the number and cumulative sprout length to levels comparable to those in control cells. Similarly, we observed that reducing *SQLE* expression in itself disrupts the organization of adherens junctions, further highlighting the need for the tight regulation of SQLE levels (Figures S4C–S4E). Different from the sprouting experiments, the knockdown of *SQLE* in *MARCHF6*-silenced cells did not rescue adherens junction organization. This could suggest that the role of MARCH6 in establishing cell-cell junctions is more complex and may depend on other factors as well. In aggregate, our results demonstrate that EC-driven sprouting is highly sensitive to SQLE activity and indicate that SQLE abundance must be tightly controlled to maintain adequate EC function. Owing to its ability to couple cellular cholesterol levels to the proteasomal degradation of SQLE, the E3 ubiquitin ligase MARCH6 plays a critical role in fine-tuning SQLE activity and is therefore a previously unrecognized determinant of EC function.

DISCUSSION

The endothelium provides a dynamic, selective barrier between the vessel lumen and the surrounding tissues. Disturbances in ECs lining the blood vessels and lymphatic vessels are linked to multiple highly prevalent diseases, such as cardiovascular disease, diabetes, cancer, and lymphedema (Li et al., 2019). Our study highlights the critical role that the cholesterol synthesis pathway and its regulation play in establishing a healthy endothelium. As such, our key finding is the positioning of SQLE, a rate-limiting enzyme in the mevalonate pathway, and its post-transcriptional regulation by the E3 ubiquitin ligase MARCH6 as important determinants of endothelial junctional integrity and angiogenesis.

MARCH6 is a member of the large E3 ubiquitin ligase family that has >600 known members (Li et al., 2008; Schwartz and Ciechanover, 2009). E3 ligases are implicated in a wide array of physiological processes. Several have been demonstrated to influence the endothelium, including, among others, cullin-3, which ubiquitinates Rho-B (Kovačević et al., 2018), and MARCH3, which controls the expression of tight junction proteins (Leclair et al., 2016). Moreover, the viral MARCH family E3 ligase K5 has been shown to directly disrupt the endothelial barrier by promoting the ubiquitylation and degradation of VE-cadherin itself (Mansouri et al., 2008; Nanes et al., 2017). Our study further extends the role of the ubiquitin-proteasomal system in endothelial function by implicating the regulation of SQLE levels by MARCH6 herein. The number of established bona fide MARCH6 targets to date is limited. In addition to SQLE (Foresti et al., 2013; Zelcer et al., 2014), MARCH6 has been reported to induce the degradation of DIO2 (Zavacki et al., 2009), PLIN2 (Nguyen et al., 2019), and, more recently, lanosterol-14 α-demethylase (Scott et al., 2020). Our results demonstrate that the knockdown of *SQLE* in *MARCHF6*-silenced cells fully rescues angiogenic sprouting. While we cannot formally rule out the involvement of other targets, this finding points toward the regulation of SQLE by MARCH6 as a prominent determinant in this process. The specific SQLE inhibitor, NB-598 (Horie et al., 1990) reversed cholesterol accumulation in MARCH6-deficient ECs, adjusting cholesterol biosynthesis may underlie the role of the MARCH6-SQLE axis in angiogenesis. We observed that the loss of SQLE function in itself led to a marked decrease in angiogenic capacity, as was also reported in a recent study (Rohlenova et al., 2020). Elegantly, using single-cell RNA sequencing (RNA-seq) and bioinformatic analysis, this study identified increased *SQLE* expression in murine lung tumor ECs, suggesting a role for SQLE in tumor-associated neovascularization. Our finding that not only loss but also gain of SQLE function, either by ectopic overexpression or by *MARCHF6* silencing, impairs angiogenesis further highlights the prominent role of SQLE in governing EC cholesterol homeostasis.

Our study adds to the understanding of how cholesterol influences EC-driven angiogenesis. Several studies have recently examined the role of cholesterol efflux in this process. Fang et al. (2013) reported that increasing ApolipoproteinA-1-binding protein (AIBP)-mediated cholesterol efflux reduced cholesterol levels led to the impaired dimerization of VEGF receptor 2 (VEGFR2) and a reduced sprouting angiogenesis (Gu et al., 2019). Similarly, promoting cholesterol efflux by the pharmacologic activation of the liver-X-receptor (LXR) pathway inhibits endothelial migration, proliferation, and angiogenesis in a cholesterol- and VEGFR2-dependent manner (Noghero et al., 2012). Reciprocally, inhibiting cholesterol efflux by silencing the endothelial cholesterol transporters *Abca1* or *Abgc1* increased cellular cholesterol content and enhanced sprouting angiogenesis (Fang et al., 2013; Gu et al., 2019; Westerterp et al., 2016). Our finding that both gain and loss of SQLE function impair angiogenesis can be reconciled with the above studies by postulating that to support angiogenesis, the cellular cholesterol pool must remain within a narrow range. Different from cholesterol efflux, the role of cholesterol biosynthesis in angiogenesis is less clear. Studies with statins, which inhibit the rate-limiting enzyme 3-hydroxy-3-methylglutaryl-coenzyme A reductase (HMGCR), have reported conflicting dose-dependent biphasic effects in both inhibiting and promoting angiogenesis (Dulak and Józkowicz, 2005; Maione et al., 2015; Weis et al., 2002). Our study demonstrates a clear role for the cholesterol

(G) Quantification of the filipin intensity of the images in (F). Each bar shows the mean filipin intensity ± SE; the signal was corrected to the background and normalized to shCtrl. n = 3, ***p < 0.001.

(H) HUVECs were transduced with shCtrl or *shMARCHF6* #2 and subsequently with shCtrl or sh*SQLE*. Total cell lysates were immunoblotted as indicated, and a representative immunoblot is shown. n = 3.

(I) Representative phase-contrast images of sprouting spheroids from cells immunoblotted in (H). A total of 57/50/36/49 spheroids from the (Ctrl/Ctrl)/(shCtrl/*shSQLE*)/(*shMARCHF6* #2/Ctrl)/(*shMARCHF6* #2/SQLE) groups, respectively, were analyzed.

(J)Boxplot showing the median (±upper and lower quartiles) of the number of sprouts in the spheroid-based angiogenesis assays. Whiskers show the minimum and maximum values. n = 4, ***p < 0.001.

(K) Boxplot showing the median (±upper and lower quartiles) of the cumulative sprout length in the spheroid-based angiogenesis assays. Whiskers show the minimum and maximum values. n = 4, ***p < 0.001.

biosynthetic rate-limiting enzyme SQLE in angiogenesis and also in establishing intact cell-cell junctions in ECs. However, in contrast to angiogenic sprouting, ablation of SQLE does not rescue disorganized adherens junctions in *MARCHF6*-silenced ECs. One possibility is that other MARCH6 targets or regulated processes may influence junctional integrity. We found that cellular membrane order, as assessed by laurdan imaging, was reduced in ECs when MARCH6 was absent. This was somewhat unexpected, as it is generally thought that an increase in membrane cholesterol content typically increases membrane order (Jay and Hamilton, 2017; Owen et al., 2011). While the molecular underpinning of the reduced membrane order is unclear at present, we speculate that this may contribute to the disturbed adherens junctions and membrane dynamics in *MARCHF6*-silenced ECs.

Finally, several recent studies have highlighted SQLE as an oncogene and as a potential therapeutic target in liver cancer (Cirmena et al., 2018; Liu et al., 2018). Similar studies have identified SQLE inhibition as a metabolic vulnerability in neuroendocrine cancers and in anaplastic large cell lymphoma, although in these settings it seems that the accumulation of squalene itself and not attenuated cholesterol biosynthesis underlies, at large, the antitumor response (Garcia-Bermudez et al., 2019; Mahoney et al., 2019). Angiogenesis is required to support tumor growth by ensuring the supply of nutrients and is hence considered an anticancer therapeutic target (Li et al., 2019). As such, our study extends the potential use of SQLE inhibition by suggesting that it may offer an approach to limit pathologic angiogenesis. The availability of established small-molecule SQLE inhibitors warrants exploring this idea, as well as the possibility that MARCH6 regulates angiogenesis *in vivo*. In summary, our study reveals an unrecognized link between cholesterol synthesis and endothelial function that is governed by the MARCH6-SQLE nexus.

STAR★METHODS

Detailed methods are provided in the online version of this paper and include the following:

- KEY RESOURCES TABLE
- RESOURCE AVAILABILITY
  - Lead contact
  - Materials availability
  - Data and code availability
- EXPERIMENTAL MODEL AND SUBJECT DETAILS
- METHOD DETAILS
  - Generation of lentiviral particles and transduction of cell lines
  - Immunofluorescence and cell staining
  - Fluorescence Microscopy
  - Scratch Assay
  - Electron Microscopy
  - Cell fractionation
  - Immunoblot analysis
  - RNA isolation and real-time quantitative PCR (RT-qPCR)
  - LDL uptake by flow cytometry analysis
  - Lipid extraction and cholesterol level measurement
  - ECIS
  - Sprouting angiogenesis assay
- QUANTIFICATION AND STATISTICAL ANALYSIS

SUPPLEMENTAL INFORMATION

Supplemental Information can be found online at https://doi.org/10.1016/j.celrep.2020.107944.

ACKNOWLEDGMENTS

We thank the members of the Zelcer and Huveneers groups, Irith Koster, Benjamin Pasquiou, and Diederick Stellingsma for their comments. J.M.E.T. is supported by an Amsterdam UMC (AMC) PhD fellowship. A.L. is supported by a Dekker grant from the Dutch Heart Foundation (2016T015). S.H. is supported by a Vidi grant from the Netherlands Organization of Scientific Research (NWO; 016.156.327). N.Z. is an Established Investigator of the Dutch Heart Foundation (2013T111) and is supported by a research grant from the Ara Parseghian Medical Research Fund, an ERC Consolidator grant (617376) from the European Research Council, and a Vici grant from the NWO (016.176.643).

AUTHOR CONTRIBUTIONS

The study was jointly conceived and designed by I.K., P.L.H., J.M.E.T., M.M.v.d.S., S.H., and N.Z. All of the authors contributed extensively to the work presented in this article. J.M.E.T., M.M.v.d.S., M.v.d.B., N.M.v.L., M.M., and A.L. designed, performed, collected data, and analyzed the cell-based experiments. E.S. and N.N.v.d.W. performed and analyzed the electron microscopy experiments. J.M.E.T., M.M.v.d.S., S.H., and N.Z. wrote the paper. All of the authors discussed the results and implications and commented on the manuscript.

DECLARATION OF INTERESTS

The authors declare no competing interests.

Received: March 16, 2020
Revised: June 23, 2020
Accepted: July 1, 2020
Published: August 4, 2020

REFERENCES

Baumgartner, W., Weth, A., Gutberlet, J., Harms, G., and Groschner, K. (2014). Localization of VE-cadherin in plasmalemmal cholesterol rich microdomains and the effects of cholesterol depletion on VE-cadherin mediated cell-cell adhesion. Biochim. Biophys. Acta *1841*, 1725–1732.

Bentley, K., Franco, C.A., Philippides, A., Blanco, R., Dierkes, M., Gebala, V., Stanchi, F., Jones, M., Aspalter, I.M., Cagna, G., et al. (2014). The role of differential VE-cadherin dynamics in cell rearrangement during angiogenesis. Nat. Cell Biol. *16*, 309–321.

Brezovjakova, H., Tomlinson, C., Mohd Naim, N., Swiatlowska, P., Erasmus, J.C., Huveneers, S., Gorelik, J., Bruche, S., and Braga, V.M.M. (2019). Junction Mapper is a novel computer vision tool to decipher cell-cell contact phenotypes. eLife *8*, e45413.

Carmeliet, P., and Jain, R.K. (2011). Molecular mechanisms and clinical applications of angiogenesis. Nature *473*, 298–307.

Chua, N.K., Hart-Smith, G., and Brown, A.J. (2019). Non-canonical ubiquitination of the cholesterol-regulated degron of squalene monooxygenase. J. Biol. Chem. *294*, 8134–8147.

Cirmena, G., Franceschelli, P., Isnaldi, E., Ferrando, L., De Mariano, M., Ballestrero, A., and Zoppoli, G. (2018). Squalene epoxidase as a promising metabolic target in cancer treatment. Cancer Lett. *425*, 13–20.

Conway, D.E., and Schwartz, M.A. (2013). Flow-dependent cellular mechanotransduction in atherosclerosis. J. Cell Sci. *126*, 5101–5109.

Cruys, B., Wong, B.W., Kuchnio, A., Verdegem, D., Cantelmo, A.R., Conradi, L.-C., Vandekeere, S., Bouché, A., Cornelissen, I., Vinckier, S., et al. (2016). Glycolytic regulation of cell rearrangement in angiogenesis. Nat. Commun. *7*, 12240.

Davignon, J., and Ganz, P. (2004). Role of endothelial dysfunction in atherosclerosis. Circulation *109* (*23, Suppl 1*), III27–III32.

De Bock, K., Georgiadou, M., Schoors, S., Kuchnio, A., Wong, B.W., Cantelmo, A.R., Quaegebeur, A., Ghesquière, B., Cauwenberghs, S., Eelen, G., et al. (2013). Role of PFKFB3-driven glycolysis in vessel sprouting. Cell *154*, 651–663.

Dejana, E., and Orsenigo, F. (2013). Endothelial adherens junctions at a glance. J. Cell Sci. *126*, 2545–2549.

Dorland, Y.L., Malinova, T.S., van Stalborch, A.-M.D., Grieve, A.G., van Geemen, D., Jansen, N.S., de Kreuk, B.-J., Nawaz, K., Kole, J., Geerts, D., et al. (2016). The F-BAR protein pacsin2 inhibits asymmetric VE-cadherin internalization from tensile adherens junctions. Nat. Commun. *7*, 12210.

Dulak, J., and Józkowicz, A. (2005). Anti-angiogenic and anti-inflammatory effects of statins: relevance to anti-cancer therapy. Curr. Cancer Drug Targets *5*, 579–594.

Fang, L., Choi, S.-H., Baek, J.S., Liu, C., Almazan, F., Ulrich, F., Wiesner, P., Taleb, A., Deer, E., Pattison, J., et al. (2013). Control of angiogenesis by AIBP-mediated cholesterol efflux. Nature *498*, 118–122.

Foresti, O., Ruggiano, A., Hannibal-Bach, H.K., Ejsing, C.S., and Carvalho, P. (2013). Sterol homeostasis requires regulated degradation of squalene monooxygenase by the ubiquitin ligase Doa10/Teb4. eLife *2*, e00953.

Garcia-Bermudez, J., Baudrier, L., Bayraktar, E.C., Shen, Y., La, K., Guarecuco, R., Yucel, B., Fiore, D., Tavora, B., Freinkman, E., et al. (2019). Squalene accumulation in cholesterol auxotrophic lymphomas prevents oxidative cell death. Nature *567*, 118–122.

Giannotta, M., Trani, M., and Dejana, E. (2013). VE-cadherin and endothelial adherens junctions: active guardians of vascular integrity. Dev. Cell *26*, 441–454.

Gill, S., Stevenson, J., Kristiana, I., and Brown, A.J. (2011). Cholesterol-dependent degradation of squalene monooxygenase, a control point in cholesterol synthesis beyond HMG-CoA reductase. Cell Metab. *13*, 260–273.

Gu, Q., Yang, X., Lv, J., Zhang, J., Xia, B., Kim, J.-D., Wang, R., Xiong, F., Meng, S., Clements, T.P., et al. (2019). AIBP-mediated cholesterol efflux instructs hematopoietic stem and progenitor cell fate. Science *363*, 1085–1088.

Hahn, C., and Schwartz, M.A. (2009). Mechanotransduction in vascular physiology and atherogenesis. Nat. Rev. Mol. Cell Biol. *10*, 53–62.

Hansson, G.K., and Libby, P. (2006). The immune response in atherosclerosis: a double-edged sword. Nat. Rev. Immunol. *6*, 508–519.

Hassink, G., Kikkert, M., van Voorden, S., Lee, S.-J., Spaapen, R., van Laar, T., Coleman, C.S., Bartee, E., Früh, K., Chau, V., and Wiertz, E. (2005). TEB4 is a C4HC3 RING finger-containing ubiquitin ligase of the endoplasmic reticulum. Biochem. J. *388*, 647–655.

Horie, M., Tsuchiya, Y., Hayashi, M., Iida, Y., Iwasawa, Y., Nagata, Y., Sawasaki, Y., Fukuzumi, H., Kitani, K., and Kamei, T. (1990). NB-598: a potent competitive inhibitor of squalene epoxidase. J. Biol. Chem. *265*, 18075–18078.

Horton, J.D., Shah, N.A., Warrington, J.A., Anderson, N.N., Park, S.W., Brown, M.S., and Goldstein, J.L. (2003). Combined analysis of oligonucleotide microarray data from transgenic and knockout mice identifies direct SREBP target genes. Proc. Natl. Acad. Sci. USA *100*, 12027–12032.

Ikonen, E. (2001). Roles of lipid rafts in membrane transport. Curr. Opin. Cell Biol. *13*, 470–477.

Jay, A.G., and Hamilton, J.A. (2017). Disorder Amidst Membrane Order: Standardizing Laurdan Generalized Polarization and Membrane Fluidity Terms. J. Fluoresc. *27*, 243–249.

Jin, F., Hagemann, N., Sun, L., Wu, J., Doeppner, T.R., Dai, Y., and Hermann, D.M. (2018). High-density lipoprotein (HDL) promotes angiogenesis via S1P3-dependent VEGFR2 activation. Angiogenesis *21*, 381–394.

Korff, T., and Augustin, H.G. (1999). Tensional forces in fibrillar extracellular matrices control directional capillary sprouting. J. Cell Sci. *112*, 3249–3258.

Kovačević, I., Sakaue, T., Majoleé, J., Pronk, M.C., Maekawa, M., Geerts, D., Fernandez-Borja, M., Higashiyama, S., and Hordijk, P.L. (2018). The Cullin-3-Rbx1-KCTD10 complex controls endothelial barrier function via K63 ubiquitination of RhoB. J. Cell Biol. *217*, 1015–1032.

Leclair, H.M., André-Grégoire, G., Treps, L., Azzi, S., Bidère, N., and Gavard, J. (2016). The E3 ubiquitin ligase MARCH3 controls the endothelial barrier. FEBS Lett. *590*, 3660–3668.

Leichner, G.S., Avner, R., Harats, D., and Roitelman, J. (2009). Dislocation of HMG-CoA reductase and Insig-1, two polytopic endoplasmic reticulum proteins, en route to proteasomal degradation. Mol. Biol. Cell *20*, 3330–3341.

Li, W., Bengtson, M.H., Ulbrich, A., Matsuda, A., Reddy, V.A., Orth, A., Chanda, S.K., Batalov, S., and Joazeiro, C.A.P. (2008). Genome-wide and functional annotation of human E3 ubiquitin ligases identifies MULAN, a mitochondrial E3 that regulates the organelle's dynamics and signaling. PLOS ONE *3*, e1487.

Li, X., Sun, X., and Carmeliet, P. (2019). Hallmarks of Endothelial Cell Metabolism in Health and Disease. Cell Metab. *30*, 414–433.

Libby, P. (2002). Inflammation in atherosclerosis. Nature *420*, 868–874.

Liu, D., Wong, C.C., Fu, L., Chen, H., Zhao, L., Li, C., Zhou, Y., Zhang, Y., Xu, W., Yang, Y., et al. (2018). Squalene epoxidase drives NAFLD-induced hepatocellular carcinoma and is a pharmaceutical target. Sci. Transl. Med. *10*, eaap9840.

Loregger, A., Cook, E.C.L., Nelson, J.K., Moeton, M., Sharpe, L.J., Engberg, S., Karimova, M., Lambert, G., Brown, A.J., and Zelcer, N. (2015). A MARCH6 and IDOL E3 ubiquitin ligase circuit uncouples cholesterol synthesis from lipoprotein uptake in hepatocytes. Mol. Cell. Biol. *36*, 285–294.

Loregger, A., Nelson, J.K., and Zelcer, N. (2017). Assaying Low-Density-Lipoprotein (LDL) Uptake into Cells. In Cholesterol Homeostasis, I.C. Gelissen and A.J. Brown, eds. (Springer), pp. 53–63.

Loregger, A., Raaben, M., Nieuwenhuis, J., Tan, J.M.E., Jae, L.T., van den Hengel, L.G., Hendrix, S., van den Berg, M., Scheij, S., Song, J.-Y., et al. (2020). Haploid genetic screens identify SPRING/C12ORF49 as a determinant of SREBP signaling and cholesterol metabolism. Nat. Commun. *11*, 1128. https://doi.org/10.1038/s41467-020-14811-1.

Mahoney, C.E., Pirman, D., Chubukov, V., Sleger, T., Hayes, S., Fan, Z.P., Allen, E.L., Chen, Y., Huang, L., Liu, M., et al. (2019). A chemical biology screen identifies a vulnerability of neuroendocrine cancer cells to SQLE inhibition. Nat. Commun. *10*, 96.

Maione, F., Oliaro-Bosso, S., Meda, C., Di Nicolantonio, F., Bussolino, F., Balliano, G., Viola, F., and Giraudo, E. (2015). The cholesterol biosynthesis enzyme oxidosqualene cyclase is a new target to impair tumour angiogenesis and metastasis dissemination. Sci. Rep. *5*, 9054.

Mansouri, M., Rose, P.P., Moses, A.V., and Früh, K. (2008). Remodeling of endothelial adherens junctions by Kaposi's sarcoma-associated herpesvirus. J. Virol. *82*, 9615–9628.

Meijering, E., Jacob, M., Sarria, J.C.F., Steiner, P., Hirling, H., and Unser, M. (2004). Design and validation of a tool for neurite tracing and analysis in fluorescence microscopy images. Cytometry A *58*, 167–176.

Montero-Balaguer, M., Swirsding, K., Orsenigo, F., Cotelli, F., Mione, M., and Dejana, E. (2009). Stable vascular connections and remodeling require full expression of VE-cadherin in zebrafish embryos. PLOS ONE *4*, e5772.

Nanes, B.A., Grimsley-Myers, C.M., Cadwell, C.M., Robinson, B.S., Lowery, A.M., Vincent, P.A., Mosunjac, M., Früh, K., and Kowalczyk, A.P. (2017). p120-catenin regulates VE-cadherin endocytosis and degradation induced by the Kaposi sarcoma-associated ubiquitin ligase K5. Mol. Biol. Cell *28*, 30–40.

Nguyen, K.T., Lee, C.S., Mun, S.-H., Truong, N.T., Park, S.K., and Hwang, C.-S. (2019). N-terminal acetylation and the N-end rule pathway control degradation of the lipid droplet protein PLIN2. J. Biol. Chem. *294*, 379–388.

Noghero, A., Perino, A., Seano, G., Saglio, E., Lo Sasso, G., Veglio, F., Primo, L., Hirsch, E., Bussolino, F., and Morello, F. (2012). Liver X receptor activation reduces angiogenesis by impairing lipid raft localization and signaling of vascular endothelial growth factor receptor-2. Arterioscler. Thromb. Vasc. Biol. *32*, 2280–2288.

Owen, D.M., Rentero, C., Magenau, A., Abu-Siniyeh, A., and Gaus, K. (2011). Quantitative imaging of membrane lipid order in cells and organisms. Nat. Protoc. *7*, 24–35.

Pober, J.S., Min, W., and Bradley, J.R. (2009). Mechanisms of endothelial dysfunction, injury, and death. Annu. Rev. Pathol. *4*, 71–95.

Rohlenova, K., Goveia, J., García-Caballero, M., Subramanian, A., Kalucka, J., Treps, L., Falkenberg, K.D., de Rooij, L.P.M.H., Zheng, Y., Lin, L., et al. (2020). Single-Cell RNA Sequencing Maps Endothelial Metabolic Plasticity in Pathological Angiogenesis. Cell Metab. *31*, 862–877.e14.

Schoors, S., De Bock, K., Cantelmo, A.R., Georgiadou, M., Ghesquière, B., Cauwenberghs, S., Kuchnio, A., Wong, B.W., Quaegebeur, A., Goveia, J., et al. (2014). Partial and transient reduction of glycolysis by PFKFB3 blockade reduces pathological angiogenesis. Cell Metab. *19*, 37–48.

Schwartz, A.L., and Ciechanover, A. (2009). Targeting proteins for destruction by the ubiquitin system: implications for human pathobiology. Annu. Rev. Pharmacol. Toxicol. *49*, 73–96.

Scott, N.A., Sharpe, L.J., Capell-Hattam, I.M., Gullo, S.J., Luu, W., and Brown, A.J. (2020). The cholesterol synthesis enzyme lanosterol 14α-demethylase is post-translationally regulated by the E3 ubiquitin ligase MARCH6. Biochem. J. *477*, 541–555.

Scutigliani, E.M., Scholl, E.R., Grootemaat, A.E., Khanal, S., Kochan, J.A., Krawczyk, P.M., Reits, E.A., Garzan, A., Ngo, H.X., Green, K.D., et al. (2018). Interfering with DNA decondensation as a strategy against mycobacteria. Front. Microbiol. *9*, 2034.

Sharpe, L.J., and Brown, A.J. (2013). Controlling cholesterol synthesis beyond 3-hydroxy-3-methylglutaryl-CoA reductase (HMGCR). J. Biol. Chem. *288*, 18707–18715.

Sharpe, L.J., Cook, E.C.L., Zelcer, N., and Brown, A.J. (2014). The UPS and downs of cholesterol homeostasis. Trends Biochem. Sci. *39*, 527–535.

Tan, J.T.M., Prosser, H.C.G., Vanags, L.Z., Monger, S.A., Ng, M.K.C., and Bursill, C.A. (2014). High-density lipoproteins augment hypoxia-induced angiogenesis via regulation of post-translational modulation of hypoxia-inducible factor 1α. FASEB J. *28*, 206–217.

Tan, J.M.E., Cook, E.C.L., van den Berg, M., Scheij, S., Zelcer, N., and Loregger, A. (2019). Differential use of E2 ubiquitin conjugating enzymes for regulated degradation of the rate-limiting enzymes HMGCR and SQLE in cholesterol biosynthesis. Atherosclerosis *281*, 137–142.

van der Stoel, M., Schimmel, L., Nawaz, K., van Stalborch, A.-M., de Haan, A., Klaus-Bergmann, A., Valent, E.T., Koenis, D.S., van Nieuw Amerongen, G.P., de Vries, C.J., et al. (2020). DLC1 is a direct target of activated YAP/TAZ that drives collective migration and sprouting angiogenesis. J. Cell. Sci. *133*, jcs.239947.

Vestweber, D., Winderlich, M., Cagna, G., and Nottebaum, A.F. (2009). Cell adhesion dynamics at endothelial junctions: VE-cadherin as a major player. Trends Cell Biol. *19*, 8–15.

Weis, S.M. (2008). Vascular permeability in cardiovascular disease and cancer. Curr. Opin. Hematol. *15*, 243–249.

Weis, M., Heeschen, C., Glassford, A.J., and Cooke, J.P. (2002). Statins have biphasic effects on angiogenesis. Circulation *105*, 739–745.

Westerterp, M., Tsuchiya, K., Tattersall, I.W., Fotakis, P., Bochem, A.E., Molusky, M.M., Ntonga, V., Abramowicz, S., Parks, J.S., Welch, C.L., et al. (2016). Deficiency of ATP-Binding Cassette Transporters A1 and G1 in Endothelial Cells Accelerates Atherosclerosis in Mice. Arterioscler. Thromb. Vasc. Biol. *36*, 1328–1337.

Zavacki, A.M., Arrojo E Drigo, R., Freitas, B.C., Chung, M., Harney, J.W., Egri, P., Wittmann, G., Fekete, C., Gereben, B., and Bianco, A.C. (2009). The E3 ubiquitin ligase TEB4 mediates degradation of type 2 iodothyronine deiodinase. Mol. Cell. Biol. *29*, 5339–5347.

Zelcer, N., Sharpe, L.J., Loregger, A., Kristiana, I., Cook, E.C.L., Phan, L., Stevenson, J., and Brown, A.J. (2014). The E3 ubiquitin ligase MARCH6 degrades squalene monooxygenase and affects 3-hydroxy-3-methyl-glutaryl coenzyme A reductase and the cholesterol synthesis pathway. Mol. Cell. Biol. *34*, 1262–1270.

STAR★METHODS

KEY RESOURCES TABLE

REAGENT or RESOURCE	SOURCE	IDENTIFIER
Antibodies		
VE-Cadherin (immunofluorescence)	Cayman Chemicals	160840; RRID:AB_10077705
PromoFluor-415 Phalloidin	Promokine	PK = PF415-7-01
Alexa Fluor-594 Secondary Antibody	ThermoFisher	A10474
Alexa Fluor 647 Mouse Anti-Human CD144	BD Biosciences	Clone 55-7H1; RRID:AB_10712766
β-Actin	Merck	MAB1501; RRID:AB_2223041
SQLE	Protein Tech Group	12544-1-AP; RRID:AB_2195888
VE-Cadherin (immunoblot)	Enzo Life Sciences	ALX-803-305-C100; RRID:AB_2052810
TEB4 (MARCH6)	Bethyl Laboratories	A304-171A; RRID:AB_2621420
GM130	Cell Signaling Technologies	12480; RRID:AB_2797933
Goat Anti-mouse-HRP	Life Technologies	A28177; RRID:AB_2536163
Goat Anti-rabbit-HRP	Life Technologies	A27036; RRID:AB_2536099
V5	Invitrogen	R960-25; RRID:AB_2556564
Chemicals, Peptides, and Recombinant Proteins		
DMEM 1X+GlutaMAX-1	ThermoFisher	11965092
Penicillin-Streptomycin	ThermoFisher	15140122
Stempro Accutase	ThermoFisher	A1110501
Endothelial Cell Growth Medium 2 Kit	Promocell	C-22111
DMSO	Sigma Aldrich	472301
NB598	MedChemExpress	HY-16343C
Gelatin	Sigma Aldrich	G7041
Polybrene	Santa Cruz	sc-134220
Fibronectin	Sigma Aldrich	F0895
Triton X-100	Sigma Aldrich	X100
Bovine Serum Albumin	Roche	10735086001
Filipin-III	Sigma Aldrich	F4767
HCS LipidTox Red Neutral Lipid Stain	ThermoFisher	H34476
Mowiol 4-88	Sigma Aldrich	81381
Dabco	Sigma Aldrich	290734
Paraformaldehyde	Merck	30525-89-4
Glutaraldehyde	Sigma Aldrich	G6257
EDTA	Sigma Aldrich	E6758
EGTA	Milipore	324626
Protease Inhibitor Cocktail	Sigma Aldrich	P8340
Phenylmethanesulfonylfluoride	Sigma Aldrich	78830
Digitonin	Sigma Aldrich	D141
Sodium deoxycholate	Sigma Aldrich	D6750
IGEPAL	Sigma Aldrich	I8896
RIPA Buffer	Boston BioProducts	BP-115
Dil-LDL	ThermoFisher	L3482
Methyl Cellulose (viscosity 4000 cP)	Sigma Aldrich	M0512
MTT (3-(4,5-Dimethyl-2-thiazolyl)-2,5-diphenyl-2H-tetrazolium bromide)	Merck	M2128
Collagen type I, Rat tail	IBIDI	50201

(*Continued on next page*)

Continued

REAGENT or RESOURCE	SOURCE	IDENTIFIER
Human VEGF	PeproTech	100-20
L-Cysteine	Sigma Aldrich	W326305
Critical Commercial Assays		
iScript cDNA Synthesis kit	Bio-Rad	1708890
SensiFAST SYBR® No-ROX Kit	Bioline	BIO-98050
NuPAGE 4-12% Bis-Tris Protein Gels	ThermoFisher	NP0321BOX
iBlot 2 Transfer Stacks	ThermoFisher	IB23001
ECIS cultureware 8W10E	Ibidi	72010
NuPAGE LDS Sample Buffer (4X)	ThermoFisher	NP0007
Amplex Red Cholesterol Assay Kit	ThermoFisher	A12216
Experimental Models: Cell Lines		
Human umbilical endothelial cells (HUVECs)	Lonza	C2519A
HEK293T	ATCC	CRL-11268
Oligonucleotides		
shRNA targeting *MARCH6* and *SQLE*	Table S1, this paper	N/A
Recombinant DNA		
pENTR/pTER+ (4301-1)	Addgene	17453
pLentiX1-PGK-GFP-DEST (694-6)	Addgene	Modified from 17297
pLKO	Addgene	10878
Software and Algorithms		
NeuronJ ImageJ plugin	Meijering et al., 2004	https://imagescience.org/meijering/software/neuronj/
ImageJ	N/A	https://imagej.nih.gov/ij/
Adobe illustrator CS4	N/A	N/A
GraphPad Prism 7.0a	N/A	N/A

RESOURCE AVAILABILITY

Lead contact

Further information and request for resources and reagents should be directed to and will be fulfilled by the Lead Contact, Noam Zelcer (n.zelcer@amsterdamumc.nl).

Materials availability

Plasmids generated in this study are available upon request to the Lead Contact

Data and code availability

This study did not generate/analyze any datasets or code.

EXPERIMENTAL MODEL AND SUBJECT DETAILS

Pooled primary human vascular endothelial cells (HUVEC)s (cultured up to passage six) from different donors (Lonza) were cultured in Endothelial Cell Growth Medium 2 culture medium (EGM) supplemented with the Growth Medium 2 supplement pack (Promocell) in culture flasks coated with 0,1% Gelatin in PBS (Sigma). Cell viability was determined using an MTT assay. HEK293T cells (ATCC) were cultured in Dulbecco's Medium Eagle medium with L-glutamine supplemented with 10% FCS and penicillin (100 units mL^{-1}), and streptomycin (100 μg mL^{-1}). All cells were cultured at 37°C and 5% CO_2.

METHOD DETAILS

Generation of lentiviral particles and transduction of cell lines

To silence expression of *MARCHF6* two independent shRNA sequences targeting *MARCHF6* were cloned into pENTR/pTER+ (430-1) (addgene #17453). The resulting pENTR/pTER+*shMARCHF6* constructs and the control plasmid pENTR/pTER+shLuc (w177-1)

(addgene #17472) were recombined into the pLentiX1-PGK-GFP-DEST (694-6, modified from addgene #17297). Similarly, two independent shRNAs targeting *SQLE, UBE2J2,* and scrambled control were cloned into the pLKO lentiviral vector (addgene #10878) and pooled for virus generation. For experiments with Laurdan, two other shRNA constructs targeting *MARCHF6* were cloned into the pLKO lentiviral vector, as this backbone does not encode GFP. For SQLE overexpression experiments, the open-reading frame of human SQLE (NM_003129.4) was cloned without the terminal stop codon into pDONR221 using gateway cloning. Subsequently, pDONR221-hSQLE was recombined into pLenti6.3-V5-DEST using the gateway LR reaction, resulting in pLenti6.3-SQLE-V5. For shRNA sequences see Table S1. Lentiviral particles were generated by transiently transfecting HEK293T cells with the lentiviral expression construct together with 3rd generation packaging plasmids, as previously reported (van der Stoel et al., 2020). The supernatant containing the lentiviral particles was mixed at a 5:1 ratio with EGM2 and a final concentration of 12 μg mL^{-1} polybrene (Santa Cruz), and used to transduce HUVEC cells for 16 hours. Subsequently, the medium was refreshed to EGM2.

Immunofluorescence and cell staining

For standard immunofluorescence (IF) stainings, cells were cultured on coverslips coated with 5 μg mL^{-1} human fibronectin (Sigma Aldrich). Cells were fixed by a 10-minute incubation with 4% paraformaldehyde in PBS++ (PBS with 1 mM $CaCl_2$ and 0,5 mM $MgCl_2$). Fixed cells were permeabilized for 5 minutes with 0,5% Triton X-100 in phosphate buffered saline (PBS) and subsequently blocked for 30 minutes in 2% bovine serum albumin (BSA) in PBS. Primary and secondary antibodies were diluted in 0,5% BSA in PBS and incubated for 45 minutes for immunostainings. Between each step the fixed cells were washed thrice with 0,5% BSA in PBS. VE-cadherin was visualized with a rabbit polyclonal anti-VE-cadherin (Cayman Chemical, Cat # 160840, 1:200), and F-actin with PromoFluor-415 Phalloidin (promokine, Cat # PK = PF415-7-01, 1:200). Secondary antibodies coupled to Alexa Fluor-594 were purchased from Invitrogen and used at a 1:250 dilution. For filipin (Sigma) and LipidTOX (ThermoFisher) stainings, fixed cells were permeabilized for 10 minutes with PBS supplemented with 0,05% Triton X-100 and 3% BSA. Subsequently, cells were washed thrice with PBS and neutral lipids were stained with LipidTOX Red Neutral Lipid Stain (ThermoFisher). Nuclei were counterstained with 4′,6-diamidino-2-phenylindole (DAPI). Filipin III, a dye that specifically stains free cholesterol was used at a concentration of 25 μg mL^{-1} to stain coverslips for free cholesterol in cells (Sigma) in PBS for 30 minutes in the dark. The Laurdan staining protocol was done as reported (Owen et al., 2011). Briefly, the cells were washed with warm PBS and the medium was replaced by 5 μM Laurdan in serum-free EGM2. The cells were incubated for 30 minutes at 37°C and 5% CO_2, and subsequently washed and fixed with 4% PFA. After staining, the coverslips were washed thrice with PBS and then mounted in Mowiol4-88/DABCO solution (Sigma).

Fluorescence Microscopy

For widefield microscopy of HUVECs a NIKON Eclipse TI equipped with a lumencor SOLA SE. II light source, 60x 1.49 NA Apo TIRF (oil) objective and Andor Zyla 4.2 plus sCMOS camera and standard DAPI, GFP, mCherry or Cy5 filter cubes (NIKON) was used. For time lapse imaging, Alexa Fluor 647 Mouse Anti-Human CD144 (Clone 55-7H1, BD Biosciences) was diluted 1:500 in EGM2 and added to HUVECs transduced with shCtrl, *shMARCHF6*#1 or *shMARCHF6*#2. Frames were taken every 30 s for ~3 hours. Filipin fluorescence was assessed with a Zeiss Axioplan-2 microscope and camera, using a 63x objective (Carl Zeiss). Laurdan fluorescence was assessed using a Leica SP8X confocal microscope, using an excitation wavelength of 405 nm and spectral analysis of emission at 408-460 and 470-530 nm. PMT gains were kept constant throughout experiments, the Generalized Polarization value (GP) was quantified as described, and the pseudo colored images were generated using the provided ImageJ macro (Owen et al., 2011). To quantitatively and objectively analyze VE-cadherin-based junctions the Junction Mapper tool applied to the raw imaging data was used (Brezovjakova et al., 2019). Images were enhanced for display with an unsharp mask filter and adjusted for brightness/contrast. Filipin and LipidTOX signal was quantified by measuring the average intensity of three equal areas per image and subtracting the background. All image analysis and quantification were done in ImageJ.

Scratch Assay

For the scratch assay, HUVECs were plated on 24-wells plates coated with 5 μg ml^{-1} fibronectin. Using a 200 μl pipette point, two perpendicular scratches were made. Cells were washed twice with PBS^{2+} and subsequently, cultured in EGM-2 with 2 μg ml^{-1} Mitomycin-C or DMSO (vehicle). Cells were mounted on an inverted NIKON Eclipse Ti2 microscope, with an Okolab cage incubator and humidified CO_2 gas chamber set to 37°C and 5% CO_2. Wound healing was imaged for 12-16 hours with a 10 minute time interval using a 10x CFI achromat DL dry objective (NA 0.25) and an Andor Zyla 4.2 plus sCMOS camera. Images were adjusted for brightness and contrast and enhanced for display using an unsharp mask filter in ImageJ. The area of wound closure was analyzed using the freehand tool in ImageJ.

Electron Microscopy

Sample preparation and imaging was done as previously reported (Scutigliani et al., 2018). Cells were plated on 5 μg mL^{-1} fibronectin-coated glass coverslips and allowed to adhere for 24 hours. Subsequently, cells were fixed with 4% paraformaldehyde (Merck) and 1% Glutaraldehyde (Sigma) in 0,1 M phosphate buffer. After washing with phosphate buffer, the cells were post-fixed with 1% OsO_4 in water. Next, the specimens were dehydrated in an ethanol series and embedded in epoxy resin (LX112). Ultrathin (70 nm) sections were cut with a diamond knife (Diatome) using a Leica UC6 ultramicrotome, collected on formvar-coated Copper grids and counterstained with uranyl acetate and lead citrate. All samples were examined using a FEI Tecnai T12 transmission electron microscope at the Electron Microscopy Centre Amsterdam.

Cell fractionation

Cell fractionation was performed in a protocol adapted from Leichner et al. (2009). The cells were washed twice with PBS, detached from the plates by scraping in ice cold PBS and collected in a centrifuge tube. The cell suspension was centrifuged 10 minutes at 500 x g at 4°C and the pellet was dissolved in solution 1 (PBS, supplemented with 5 mM EDTA, 5 mM EGTA, 2 mM phenylmethanesulfonylfluoride, protease inhibitor cocktail (AEBSF at 1,04 mM, Aprotinin at 800 nM, Bestatin at 40 μM, E-64 at 140 μM, Leupeptin at 20 μM and Pepstatin A at 150 μM, obtained from Sigma), and 0.025% digitonin for 1 hour at 4°C. Subsequently, the sample was centrifuged at 4°C for 30 minutes at 16.000 x g. The supernatant was taken off (soluble fraction), and the pellet (membrane fraction) was solubilised in solution 2 (solution 1 + 1% Na-deoxycholate and 1% IGEPAL) by rotation at 4°C for 1 hour. Before immunoblot analysis, the fractions were cleared by centrifugation for 10 minutes at 16.000 x g and the supernatant was prepared for SDS-PAGE separation by adding LDS Sample Buffer (ThermoFischer), and warming at 37°C for 10 minutes.

Immunoblot analysis

Cells were lysed in radio-immunoprecipitation assay (RIPA) buffer (150 mM NaCl, 1% Nonidet P-40, 0.1% sodium deoxycholate, 0,1% SDS, 100mM Tris-HCl, pH 7,4) supplemented with 2 mM phenylmethanesulfonylfluoride and protease inhibitor cocktail (Sigma). The lysates were cleared by centrifugation at 4°C for 10 minutes at 16.000 × g. Proteins were separated on NuPAGE Novex 4%–12% Bis-Tris gels and transferred to nitrocellulose membranes (ThermoFischer). Immunoblot analysis was performed using the following antibodies: β-actin (Merck MAB1501, 1:10000), SQLE (Protein Tech Group 12544-1-AP, 1:1000), V5 (Invitrogen R960-25, 1:1000), VE-cadherin (Enzo Life Sciences ALX-803-305-C100, 1:1000), and TEB4 (MARCH6) (Bethyl Laboratories A304-171A, 1:500), GM130 (Cell signaling technologies 12480, 1:1000). Secondary HRP-conjugated antibodies (Zymed Laboratories) were used and visualized with chemiluminescence on a Fuji LAS4000 (GE Healthcare). Unless indicated, blots shown are representative of at least 3 independent experiments with similar results.

RNA isolation and real-time quantitative PCR (RT-qPCR)

RNA was isolated from cells using the Direct-zol RNA miniprep kit (Zymo Research), and cDNA was generated using the iScript reverse transcription reagent (BioRad). SensiFAST SYBR (Bioline) was used for real-time quantitative PCR (RT-qPCR). Measurements were performed on a LightCycler 480 II system (Roche) and gene expression was normalized to the expression level of 36B4. Primer sequences are available upon request.

LDL uptake by flow cytometry analysis

Cellular LDL uptake was measured as previously reported by Loregger et al. (2017). Briefly, HUVECs were plated at 50.000 cells per well in a 96-wells plate. The following day, the cells were washed with PBS and incubated for 2,5 hours with 5 $\mu g\ mL^{-1}$ Dil-labeled LDL (ThermoFischer), dissolved in EGM-LPDS. After incubation, the cells were washed twice with PBS and detached with StemPro Accutase (ThermoFischer) for 5 minutes at 37°C. The cells were washed 1x in fluorescence activated cell sorting (FACS) buffer (PBS, supplemented with 2 mM EDTA and 0,1% BSA), and after decanting the supernatant, the cells were fixed in 4% paraformaldehyde in PBS for 10 minutes. Subsequently, cells were washed in FACS buffer, taken up in FACS buffer and subjected to flow cytometry on a Beckman Coulter CytoFLEX machine. Viable, single cells were gated, and Dil-LDL signal was measured in the PE-channel (excitation 561 nm, bandpass filter 585/42 nm). Cells incubated in EGM-LPDS without Dil-LDL were used for background subtraction.

Lipid extraction and cholesterol level measurement

A detergent-free lipid-extraction was performed by collecting 1×10^6 cells per sample in glass tubes on ice. Briefly, cells were washed twice in cold PBS and centrifuged for 5 minutes at 300 x g. The pellet was directly resuspended in 2 mL of a 2:1 chloroform/methanol mixture, vortexed for 30 s and rotated at 4°C for 24 hours. Subsequently, 650 μL of H_2O was added, the sample vortexed and then centrifuged for 5 minutes at 450 x g. The lower lipid-containing phase was carefully transferred to new glass tubes and evaporated. The resulting lipid pellet was dissolved in 1x Amplex Red reaction buffer for 30 minutes at 37°C. The cholesterol content was measured using the Amplex Red Cholesterol Assay Kit (ThermoFisher) according to the manufacturer's instructions using a BioTEK Synergy HT Multi-Detection plate reader.

ECIS

Electric cell-substrate impedance sensing was used to analyze endothelial barrier function, as previously reported (Dorland et al., 2016). Electrode arrays (8W10E; Applied Biophysics) were treated with 10 mM L-cysteine (Sigma) for 15 minutes at 37°C. After washing with 0,9% NaCl the arrays were coated with 5 $\mu g\ mL^{-1}$ fibronectin in 0,9% NaCl for 1 hour at 37°C. Subsequently, 1×10^5 cells were seeded on the arrays and the impedance was measured during monolayer formation at 4 kHz using the ECIS model ZTheta (Applied BioPhysics).

Sprouting angiogenesis assay

For sprouting angiogenesis assays HUVECs were resuspended in EGM-2 medium containing 0.1% methylcellulose (4.000 cP, Sigma). To form spheroids 750 cells per 100 μl methylcellulose medium were seeded in wells of a U-bottom-shaped 96-wells plate and incubated for 16 hours. Spheroids were collected and resuspended in 1,7 $mg\ mL^{-1}$ collagen Type I rat tail mixture (IBIDI), plated in

a glass-bottomed 96 well plate and incubated at 37°C and 5% CO_2. Following polymerization of the collagen gel, spheroids were stimulated with 50 ng ml^{-1} VEGF (PeproTech) to induce sprouting for 16 hours, as described previously (Korff and Augustin, 1999). Images were taken on an EVOS M7000 imaging system, 10 x objective (ThermoFischer), and enhanced for display with an unsharp mask filter and adjusted for brightness/contrast in ImageJ. Sprouting number and length was analyzed using the ImageJ plugin NeuronJ (Meijering et al., 2004).

QUANTIFICATION AND STATISTICAL ANALYSIS

Data was analyzed with Microsoft Excel and Statistical analysis was performed using the Prism software (Graphpad V6). All bar graphs represent the mean ± SE. Outliers were removed using the ROUT method. A Student's t test was used when 2 groups were compared. Where 2 or more groups were compared to the control, One-way Analysis of Variance (ANOVA) was used in combination with a Holm-sidak test for multiple comparison, after the values passed the D'Agostino-Pearson normality test. *p* values are indicated by asterisks and defined as *p < 0,05, **p < 0,01 and ***p < 0,001.